ACS ENVIRONMENTAL Au
AN OPEN ACCESS JOURNAL OF THE AMERICAN CHEMICAL SOCIETY

pubs.acs.org/environau
Article

Haloacetonitriles Induce Structure-Related Cellular Toxicity Through Distinct Proteome Thiol Reaction Mechanisms

Published as part of ACS Environmental Auspecial issue"2024 Rising Stars in Environmental Research".

Kirsten Yeung, Linna Xie, Pranav Nair, and Hui Peng*

Cite This: *ACS Environ. Au* 2025, 5, 101−113
Read Online

ACCESS | Metrics & More | Article Recommendations | Supporting Information

ABSTRACT: Haloacetonitriles (HANs) are a class of toxic drinking water disinfection byproducts (DBPs). However, the toxicity mechanisms of HANs remain unclear. We herein investigated the structure-related in vitro toxicity of 6 representative HANs by utilizing complementary bioanalytical approaches. Dibromoacetonitrile (DBAN) displayed strong cytotoxicity and Nrf2 oxidative stress responses, followed by monohalogenated HANs (monoHANs) while other polyhalogenated HANs (polyHANs) exhibited little toxicity. Activity based protein profiling (ABPP) revealed that toxic HANs adduct to human proteome thiols, supporting thiol reactivity as the primary toxicity mechanism for HANs. By using glutathione (GSH) as a thiol surrogate, monoHANs reacted with GSH via S_N2 while polyHANs reacted through ultrafast addition reactions. In contrast, DBAN generated an unexpected fully debrominated product and glutathione disulfide (GSSG). The unique reaction of DBAN with GSH was found to be mediated by radicals which was supported by electron paramagnetic resonance (EPR) spectroscopy and by radical trapping reagent reaction quenching. Shotgun proteomics further revealed that monoHANs and DBAN adducted to proteome thiols in live cells forming dehalogenated adducts. Multiple antioxidant proteins, SOD1, CSTB, and GAPDH, were adducted by toxic HANs at specific cysteine residues. This study highlights the structurally selective toxicity of HANs in human cells, which are attributed to their distinct reactions with proteome thiols.

KEYWORDS: *haloacetonitrile, oxidative stress, thiol reactivity, radical reaction, proteomics*

INTRODUCTION

Disinfection by products (DBPs) have long been associated with various adverse health outcomes including bladder cancer.[1−4] Of the >700 DBPs discovered,[5−7] only 2 classes, trihalomethanes (THMs) and haloacetic acids (HAAs) are regulated in Canada.[8,9] However, unregulated nitrogenous-DBPs[10,11] are considerably more toxic than the regulated THMs,[12] and urgently need more attention. In particular, haloacetonitriles (HANs) are a class of nitrogenous-DBPs found commonly in disinfected drinking water.[13−16] HANs have been reported to be more cytotoxic and genotoxic than HAAs by 2 orders of magnitude.[17] Although their concentrations are lower than regulated HAAs and THMs,[18] HANs, particularly dibromoacetonitrile (DBAN), have been highlighted as one of the possible drivers of DBP toxicity in drinking water.[11,17,19] In 2022, the US EPA's Contaminant Candidate List 5 included HANs for the first time, including dichloroacetonitrile (DCAN) and DBAN.[20] Despite the mounting evidence, HANs remain unregulated in the Americas, therefore necessitating more toxicity research on HANs to better understand their potential health effects.

Although HANs have similar structures, the orally administered rat LD_{50} values of HANs exhibit *a* > 7-fold variation merely through the alteration of their halogen functionality.[21−23] The structurally selective toxicity of HANs have also been well documented by in vitro testing. For instance, Lin et al. found that DBAN exhibited the strongest alkylating ability on a DNA surrogate compared to bromochloroacetonitrile (BCAN), chloroacetonitrile (CAN), DCAN and trichloroacetonitrile (TCAN).[24] In another study, DBAN showed the highest genotoxicity and cytotoxicity within 5 tested HANs in *Salmonella typhimurium*.[25] Paralleling these results, DBAN and most monoHANs were found to be highly cytotoxic and genotoxic in Chinese hamster ovary (CHO) cells but polychlorinated HANs like TCAN and DCAN exhibited

Received: July 30, 2024
Revised: November 15, 2024
Accepted: November 27, 2024
Published: December 3, 2024

little toxicity.[17] Together, these results highlighted the structurally selective toxicity of HANs and the generally strong toxicity of DBAN, but their toxicity mechanism remains unclear.

The toxicity of DBPs has long been correlated with their ability to react with thiols such as *N*-acetyl cysteine.[26] A recent study further confirmed that thiol-reactive DBPs in water extracts primarily drive Nrf2-mediated oxidative stress in human cells, through chemical sequestration by glutathione (GSH).[27] Specifically, the cellular toxicity of haloacetamides and haloacetic acids have been linked to their capacity to modify protein cysteine residues through S_N2 reactions.[28,29] Compared to well studied haloacetamides and haloacetic acids,[28,29] a few studies found that HANs can react with proteome thiols via both S_N2 and addition reactions, depending on the number and type of halogens.[26,27,29,30] This demonstrates the complicated toxicity mechanism of HANs compared to well-studied DBPs, which highlights the necessity to explore HAN structure-related toxicity mechanisms in depth.

In this study, we selected 6 representative HANs with a distinct number (1−3 halogens) and type of halogens (Cl, Br, or I), to systematically illustrate their structure-related toxicity mechanisms in human cells. We focused on cytotoxicity and Nrf2-mediated oxidative stress as these are some of the most studied toxicity end points for DBPs.[31−34] We integrated multiple bioanalytical strategies including activity-based protein profiling (ABPP), high-resolution mass spectrometry (HRMS), electron paramagnetic resonance (EPR) spectroscopy, and shotgun proteomics to explore HAN-thiol reaction mechanisms acellularly and cellularly. Using molecular toxicology, we discovered that the cellular toxicity of HANs is governed by their unique chemical structures and mediated by their distinct proteome thiol reaction pathways.

MATERIALS AND METHODS

Chemicals and Reagents

DBAN standard (94% purity) was purchased from Alfa Aesar (Haverhill, MA, USA). All other HAN authentic standards (97−98% purity) were obtained from Sigma-Aldrich (St. Louis, MO, USA). Iodoacetamide (IAM, 98% purity) was purchased from Sigma-Aldrich (St. Louis, MO). The IAM-fluorescein used in ABPP was sourced from Toronto Research Chemicals (Toronto, ON, CA). Cell culture reagents: fetal bovine serum, antibiotic−antimycotic solution, and Geneticin were sourced from Thermo Fisher Scientific (Ottawa, ON, CA). Dulbecco's modified Eagle's medium (DMEM—high glucose) was from Sigma-Aldrich (St. Louis, MO, USA). Stably transfected luciferase MCF7 cell lines were purchased from Signosis (Santa Clara, CA, USA). The MTT Cell Viability Assay Kit was purchased from Biotium (Fremont, CA, USA). The Nrf2 assays used the Steadylite Plus gene assay system from PerkinElmer Inc. (Waltham, MA, USA). All solvents, including methanol (MeOH) were LC−MS grade and were obtained from Thermo Fisher Scientific (Waltham, MA, USA) and Sigma-Aldrich (St. Louis, MO, USA).

Cytotoxicity and Nrf2 Assays

Cytotoxicity and Nrf2 assays were performed in accordance to previously reported protocols to measure in vitro cytotoxicity and oxidative stress responses by HANs,[27,29,35] respectively. The 3-(4,5-dimethylthiazol-2-yl)-2,5-diphenyltetrazolium bromide (MTT) assay was used to measure cytotoxicity as only living cells can transform MTT to colored formazan crystals whose measurable absorbance at 570 nm is proportional to the number of living cells within the plate as compared to control groups. In both assays, luciferase-transfected MCF7 cells were seeded on 96-well plates and were subsequently dosed with a series of concentrations of HANs (1−1000 μM for the MTT assay, 1−50 μM for the Nrf2 assay) (n = 4 replicates). Previous studies have found that combined HAN concentrations can range from 0.216−14 μg/L.[15,36,37] Other bioassay-based studies typically test using enriched (i.e., concentrated 10× or more) drinking water samples.[38] Therefore, our study utilizes HAN concentrations that are comparable to literature. All exposures occurred in DMEM high glucose, supplemented with 0.1% FBS (exposure medium) and lasted for 16 h. Methanol (v/v 0.1%) was the solvent control and iodoacetamide (IAM, 50 μM) was the positive control. After 16 h of HAN exposure, 10 μL of MTT was added to all samples and controls for an additional 4 h. The formazan crystals formed after a total incubation time of 20 h were dissolved by DMSO and the samples' absorbances were measured at 570 nm using a Biotek Synergy HTX plate reader (Winooski, VT, USA).

The Nrf2 assay consists of a stably transfected luciferase human cell line to visualize increased signaling of the Nrf2-Keap1 antioxidant stress pathway. As in the MTT assay, the cells were first seeded to 96-well plates to confluency and incubated with HANs (1−50 μM) for 16 h (n = 4 replicates for each treatment group). The lower concentration range of the Nrf2 assay reflects the upper limit of cell viability as determined by the MTT assay. Previous work in our group has determined 16 h as the optimized time for this Nrf2 assay to accumulate enough signal for measurement.[27,29] After 16 h, the exposure medium was removed, cells were rinsed with phosphate buffered saline twice and 75 μL of Dulbecco's PBS containing calcium and magnesium and Steadylite buffer/substrate solution were added respectively to each replicate. Following a 15 min incubation in the dark, the chemiluminescence of each HAN concentration was measured with a BMG Labtech PHERAstar Plus HTS microplate reader (Ortenberg, BW, Germany). MeOH (v/v 0.1%) and IAM (5 μM) were used as controls.

Activity Based Protein Profiling

Activity based protein profiling (ABPP) was employed to investigate the proteome thiol reactivity of HANs as described in previous studies from our group and others.[29,39,40] In brief, MCF7 cells were grown to confluency in growing medium (DMEM, high glucose, supplemented with 10% FBS, and antibiotics) prior to 2× PBS rinses and harvested with cold PBS. The cells were centrifuged (1000g, 4 °C, 10 min), resuspended in lysis buffer (500 mM NaCl, 20 mM HEPES, 1% SDS, 0.1% NP40, pH = 7.4), freeze−thawed 3 times, and sonicated with an Ultrasonic Sonifer SFX250 Cell Disruptor (Branson Ultrasonics; Danbury, CT, USA). Afterward, 50 μg of cell lysate was incubated with each HAN respectively at varying concentrations (1−50 μM) or with MeOH vehicle solvent in duplicate for 1 h at room temperature, shaking, and in the dark (n = 2 replicates). This concentration range was chosen to adequately capture the dose response and mechanism of dosed HANs to cell lysate within the experimental time frame. Actual concentrations of various DBPs within blood samples are in the ng/L range after routine household activity like drinking and washing.[41−43] Then, 50 μM of the IAM-fluorescein probe was added to each sample to react for 1 h at room temperature, shaking, and in the dark. Finally, the labeled lysates were precipitated with cold acetone and pelleted (14,000g, 4 °C, 20 min) twice. The remaining cell pellets were dried before solubilization by SDS loading buffer (50 mM Tris−HCl, 100 mM DTT, 2% SDS, 0,1% bromophenol blue, 10% glycerol 30%, and 5% β-metcaptoethanol, pH = 6.8) and imaged by SDS-PAGE gel electrophoresis. In-gel fluorescence was imaged using a GE Healthcare Life Sciences Typhoon FLA 9500 (Chicago, IL, USA) and images were processed using ImageJ.

High-Performance Liquid Chromatography−Mass Spectrometry Orbitrap Direct Infusion

Direct infusion was used to determine HAN-GSH reaction products and kinetics. 10 μM of each HAN (IAN, BAN, CAN, and DBAN) were incubated with 1 mM of GSH respectively in ammonium bicarbonate buffered solvent (pH 8.0) and injected immediately (<30 s) into a Q Exactive Hybrid Quadrupole-Orbitrap Mass Spectrometer (Thermo Fisher Scientific; Waltham, MA, USA) to visualize the

https://doi.org/10.1021/acsenvironau.4c00068
ACS Environ. Au 2025, 5, 101−113

increase of reaction products over time. TCAN and DCAN were reacted at a 1:1 (1 mM: 1 mM) ratio with GSH respectively to capture their faster reactions. Positive and negative full MS scans (100−900 m/z) at a resolution of 70,000 (at m/z 200) were obtained over a period of 450 s. The flow rate of the sample into the spectrometer was set to 10 μL/min. Maximum injection time was set to 200 ms and the maximum ion population was set to 3×10^6. Spray voltage was held at 3.0 kV, capillary temperature at 275 °C, and sheath gas at 10 L/h.

Nuclear Magnetic Resonance Spectroscopy

Nuclear magnetic resonance (NMR) acquisition was conducted on a 500/600 MHz Agilent DD2 NMR Spectrometer (Santa Clara, CA, USA). Sixteen scans were obtained for ^{1}H spectra at a 45 °C pulse angle, 1.0 s relaxation delay, and a 6.0 s acquisition time. All NMR reactions were performed in D_2O (pH 8) as GSH is insoluble in common nonpolar solvents (e.g., chloroform) and DMSO can oxidize GSH[44] which affected HAN-GSH reaction (data not shown). Reactions were incubated for 3 h at room temperature in the dark prior to acquiring NMR spectra with a 1:1 (50 mM: 50 mM) ratio of GSH/HAN (n = 2 replicates). These conditions were chosen to capture both the slower reactions between DBAN and GSH and the faster reactions between DCAN and GSH. All reaction spectra were run alongside the respective HAN control (i.e., 50 mM DBAN or 50 mM DCAN) and a GSH only control (i.e., 50 mM GSH). All NMR spectra were baseline, solvent, and phase corrected using MestreNova for comparison between different samples.

Liquid Chromatography−Mass Spectrometry

Liquid chromatography−mass spectrometry (LC−MS) was used to supplement the HAN-GSH direct infusion data. 1 mM HAN was incubated with 1 mM GSH for 3 h prior to injection onto the LC−MS (n = 3 replicates). Reactions that involved the radical quenching agent 5,5-dimethyl-1-pyrroline-N-Oxide (DMPO) were performed as follows: 1 mM DMPO was mixed with 100 μM GSH for 10 min before the addition of 10 μM DBAN or IAM, respectively. This solution was left to stand for 3 h until injection into the Vanquish UHPLC system (Thermo Fisher Scientific, Waltham, MA) coupled to a Q Exactive Hybrid Quadrupole-Orbitrap mass spectrometer (Thermo Fisher Scientific, Waltham, MA). All samples were prepared in ammonium bicarbonate buffer (pH 8). The HAN-GSH products and reagents were separated with an RP-Amide column (2.7 μm, 2.1 mm × 100 mm, Advanced Materials Technology Inc., Wilmington, DE) with 1 μL injection volume. The LC system mobile phases were 0.1% formic acid in H_2O (A) and 0.1% formic acid in MeOH (B). Over the course of 8.5 min: B was increased from 0−2% from start to 2 min, increased again to 5% by 4 min, surged to 100% by 4.5 min, and decreased to 2% at 6 min, 2% was held static until completion. The flow rate was 0.3 mL/min and the column chamber temperature was 40 °C throughout the run.

Full scans in both positive and negative ESI modes (90−1000 m/z, 70,000 resolution at m/z 200) accompanied all MS/MS scans. The ESI settings were the same as the direct infusion MS. Briefly, the S lens RF levels were set at 50.0, spray voltage was |3 kV|, capillary temperature was set to 300 °C, and vaporizer temperature was 450 °C. The maximum injection time was set at 100 ms and the maximum ion population was set to 3×10^6.

Nontarget Analysis

Nontarget analysis was conducted to identify the reaction products from the reactions between HANs and GSH. Our nontarget strategy was performed as previously described.[27,45] Briefly, MSconvert was used to convert Raw MS files to mzXML files. Our in-house R script[45] utilized the "XCMS" R package by Smith et al.[46] to detect MS peaks with tolerances of 2.5 ppm m/z. Peak features detected in HAN-GSH reactions were compared to HAN-only or GSH-only controls. Peak features with statistically significant (p < 0.05), ≥50-fold higher abundance, and $\geq 1.0 \times 10^5$ in intensity, were further selected for structure assignments.

The HAN-GSH product formulas were predicted within a mass tolerance of 5 ppm. The atom allowance for chemical formulas were set to 100 C, 200 H, 20 N, 40 O, 3 S, 3 Cl, 2 Br, and 1 I per molecule. Characteristic isotopic halogen peaks were used to further constrain the number of reasonable halogens. All assigned formulas were required to meet basic chemical criteria as described previously.[47,48] HAN-GSH formulas were predicted at confidence level 3 (known exact mass, tentative exact structure) according to the Schymanski et al. scale.[49]

Electron Paramagnetic Resonance Spectroscopy

To capture the short-lived radical species, 100 mM of 5-(diethoxyphosphoryl)-5-methyl-1-pyrroline-N-oxide (DEPMPO) or 5,5-dimethyl-1-pyrroline-N-oxide (DMPO) were incubated with 50 mM GSH and 25 mM DBAN, respectively in ammonium bicarbonate buffer (pH 8.0). After approximately 8 min of reaction time under ambient light and temperature, the sample was measured using a Bruker CW X-band ECS-EMXplus EPR Spectrometer. Each sample was tuned prior to EPR measurement as per instrument manufacturer recommendations. The typical spectrometer parameters are as follows: 300 G scan range, 3330.4 G center field, 90 s sweep time, 30 db receiver gain, 0.01 ms time constant, 1.00 G modulation amplitude, 100 kHz modulation frequency, and 20 mW microwave power. The resultant spectra were simulated by WinSim (version 0.96, NIEHS) and the hyperfine splitting constants were calculated.

Shotgun Proteomics

Shotgun proteomics was employed to detect HAN protein adducts in live adherent cells. We incubated MCF7 cells with 10 μM of HAN for 16 h prior to lysis, mirroring both the in vitro cell assay (HAN incubation) and ABPP methodology (lysis) employed for this study (n = 3 replicates). The proteomics protocol has been reported in our previous studies.[29,39] After lysis, cells were digested with trypsin and the peptides were injected into an EASY-nanoLC 1200 UHPLC ESI source tandem Q-Exactive HF-X orbitrap mass spectrometer (Thermo Fisher Scientific; Waltham, MA, USA). Samples were separated on an in-house packed C18 column (10 cm × 75 μm internal diameter packed with 3 μm Luna C18 100 Å reverse phase beads (Phenomenex; Torrance, CA, USA)). The nanoLC solvent phases were: 0.1% formic acid in H_2O (A) and 0.1% formic acid in 80:20 acetonitrile/H_2O (B). B was increased from 2−5% in the first minute, gradually ramped to 26% by 90 min, ramped to 100% at 105 min, and held at 100% for 15 min. The flow rate was held at a constant 300 nL/min.

We employed a data-dependent acquisition (DDA) top 20 method for our shotgun proteomic experiment. Full MS scan parameters were controlled as follows: a range of 350−1400 m/z, 60,000 resolution (at m/z 200), and an AGC of 3×10^6. MS/MS scans held precursor ions 1.4 m/z windows and were accumulated for 20 ms or until the AGC target (1×10^5) was reached.

Data Analysis

All graphical analyses were performed using GraphPad Prism (v7.0.4, GraphPad Software Inc., San Diego, CA). Results were considered significant if (1) the p-value <0.05 between treatment groups (i.e., HAN protein adduct m/z response) and control groups (i.e., vehicle solvent blanks) when calculated using t-test functions; (2) there is a > 10-fold difference between treatment group adducted peptide intensities; and (3) the mass response had an intensity $>10^4$. Raw proteomics data were analyzed using MaxQuant (version 2.4.10) and default parameters were used with a false discovery rate of 1% with a list of common contaminants. Tryptic peptides were derived from the Uniprot human (assessed on Sept. 7, 2023) reference proteome and used to match extracted MS/MS spectra. Proteomic data analysis was conducted on the visualization tab of Maxquant or on Microsoft Excel. To determine HAN adducts, only variable modifications were included at the cysteine site and additionally included oxidation, N-terminal acetylation, and carbamidomethyl as per default settings. Proteomic data was uploaded to MassIVE (ftp://massive.ucsd.edu/v08/MSV000095399/). Protein structures of GADPH were generated using AlphaFold due to the lack of experimentally determined structures.

https://doi.org/10.1021/acsenvironau.4c00068
ACS Environ. Au 2025, 5, 101−113

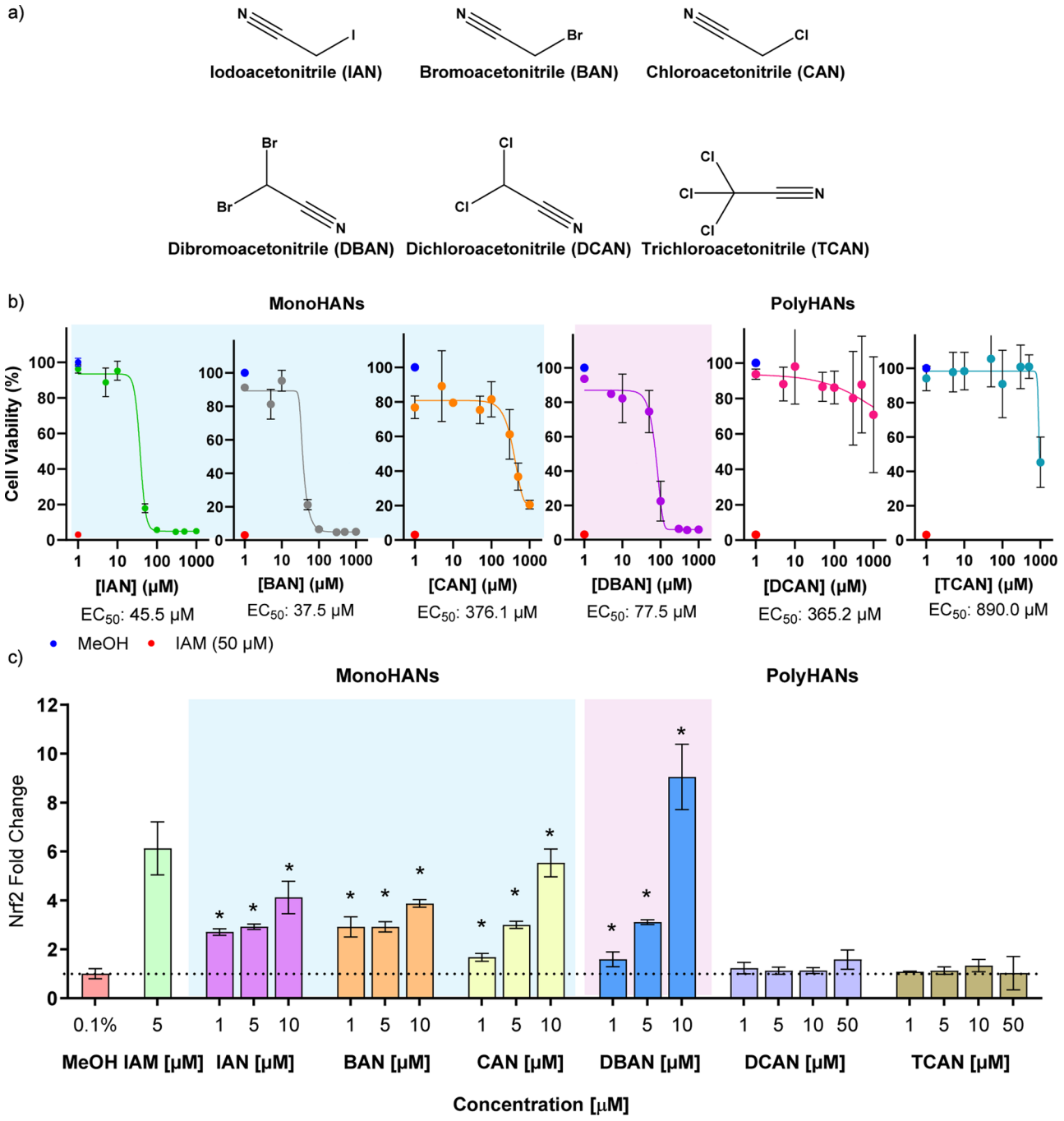

Figure 1. Selected HANs were tested for cytotoxicity and oxidative stress responses. (a) Chemical structures of the 6 HANs tested; (b) MTT assay results of 6 selected HANs ($n = 4$). EC_{50} for all tested HANs were calculated using Graphpad Prism's built in dose−response curve fitting. Controls are denoted by the legend on the bottom left. (c) Nrf2 assay results of 6 selected HANs ($n = 4$), negative control (methanol), and positive control (IAM 5 μM). Asterisks denote significantly increased Nrf2 responses ($p < 0.05$).

RESULTS AND DISCUSSION

Structure Related Cytotoxicity and Oxidative Stress Responses of HANs

Previous research has reported the potent cytotoxicity of HANs in Chinese hamster ovary (CHO) cells.[17] To determine whether this phenomenon extends to human cells, we examined 6 HANs, consisting of 3 monohalogenated (monoHANs) and 3 poly halogenated (polyHANs) HANs (structures shown in Figure 1a). The human breast cancer cell line (MCF7) was selected due to its documented sensitivity to disinfection byproducts (DBPs)[27,29] and the assay's strong correlation with other typical DBP toxicity end points.[32] Additionally, exposure to DBPs have been shown to induce increases in hormones such as progesterone and estrogen.[50,51] All monoHANs exhibited significant cytotoxicity at a concentration of 50 μM (Figure 1b), with iodoacetonitrile (IAN, 17 ± 2% cell viability, $p = 0.005$) > bromoacetonitrile (BAN, 21 ± 3% cell viability, $p = 0.01$) ≫ chloroacetonitrile (CAN, 75 ± 8% cell viability, $p = 0.01$). The observed toxicity trend was previously observed in CHO cells,[17] demonstrating the conserved toxicity effects across species and cell lines. In

https://doi.org/10.1021/acsenvironau.4c00068
ACS Environ. Au 2025, 5, 101−113

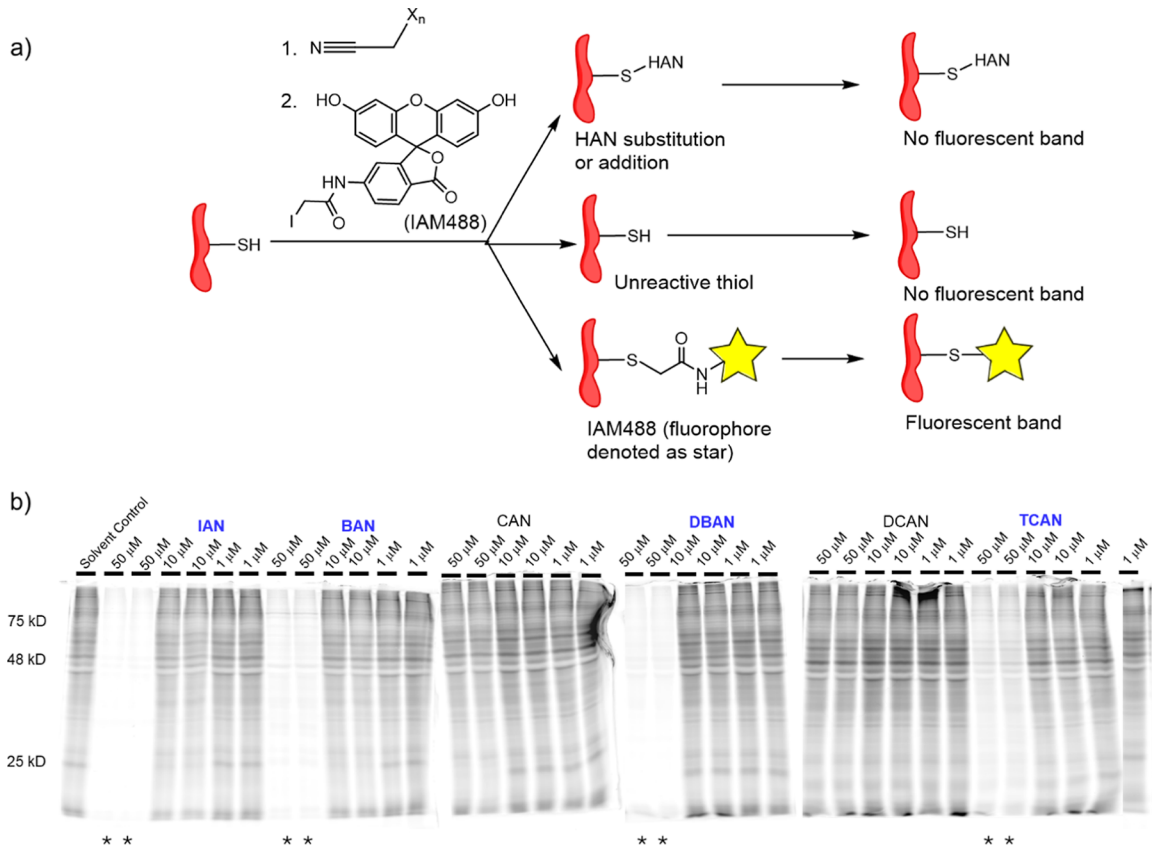

Figure 2. ABPP was used to identify proteome thiol reactivities of HANs in cell lysates. (a) ABPP workflow schematic (b) ABPP results for selected HANs (n = 2). Loss of fluorescence (gray protein bands) represent occupation by HAN on cysteine residues of lysate proteins. HANs highlighted in blue have significant HAN adduction to cysteinyl proteins; asterisks denote large amounts of thiol adduction by HANs on cell lysate proteins at various concentrations.

contrast, 2 polyHANs, DCAN and TCAN, showed no significant cytotoxicity at the tested concentrations. Interestingly, DBAN exhibited comparable cytotoxicity (e.g., 22 ± 12% cell viability at 100 μM) to monoHANs. This observation aligns with previous findings where DBAN exerted the highest cytotoxicity in CHO cells,[17] suggesting a unique mechanism of toxicity compared to other polyHANs.

To probe the mechanism of HAN cytotoxicity in human cells, we investigated their ability to induce oxidative stress which is a known pathway of DBP toxicity that may lead to downstream effects like cytotoxicity and genotoxicity.[27,29,52,53] We evaluated HAN-induced oxidative stress responses using the stably transfected Nrf2 reporter assay that has previously been used to determine oxidative stress responses by other DBPs.[27,29] Unsurprisingly, monoHANs induced significant oxidative stress at concentrations as low as 1 μM (Figure 1c) in Nrf2 cells. Contrary to its cytotoxicity data, CAN elicited significant Nrf2 responses (5.53 ± 0.57 folds) at 10 μM, surpassing those of IAN (4.12 ± 0.66 folds) and BAN (3.87 ± 0.15 folds) at the same concentration. This is likely due to the potent cytotoxicity of IAN and BAN which may mask reporter cell responses.[54] Among the 3 polyHANs, only DBAN induced Nrf2 responses. DBAN was found to induce oxidative stress at all tested concentrations (≥1 μM) and its response exceeded (50 μM, 9.05 ± 1.33 folds) that of the monoHANs. Together, this corroborates DBAN's potent cytotoxicity and possible unique toxicity pathway as opposed to its polyHAN counterparts.

Reaction of HANs with Proteome Thiols

Previous studies have postulated that the molecular initiating event for halogenated DBP toxicity in mammalian cells is via covalent adductions with protein thiols.[26,27,29,55] In particular, the Nrf2 responses of DBPs have been found to be dependent on their thiol reactivities.[27] A recent study on haloacetamides, another class of nitrogenous-DBPs, also reported the halogen-dependent cytotoxicity in CHO cells,[56] corroborated with their reactivity with proteome thiols.[29] Supported by the similarities in HAN in vitro cytotoxicity and Nrf2 profiles, we propose that HANs may also induce structure-related toxicity via a proteome thiol reaction. ABPP has previously been used to visualize the binding of DBPs to proteins in whole cell lysates,[29] which was employed herein (see the workflow in Figure 2a). To validate our hypothesis, we exposed cell lysate to varying doses of HANs for an hour to saturate all possible HAN-protein binding sites and to determine a dose−response. The IAM-fluorescein probe added after adducted to the remaining unoccupied thiol sites in the lysate. Therefore, ABPP can illustrate the proteome-wide thiol adductions of HANs with human proteome thiols by monitoring the loss of fluorescence signal in the SDS-PAGE gel. We observed a dose-dependent protein thiol reaction for monoHANs and polyHANs (Figure 2b). Among the 3 monoHANs, IAN and BAN demonstrated pronounced reactivity with proteome thiols at 50 μM, while CAN had negligible responses. This is consistent with the cytotoxicity and Nrf2 bioassay results and supports CAN's diminished S_N2 reactivity compared to its I-

https://doi.org/10.1021/acsenvironau.4c00068
ACS Environ. Au 2025, 5, 101−113

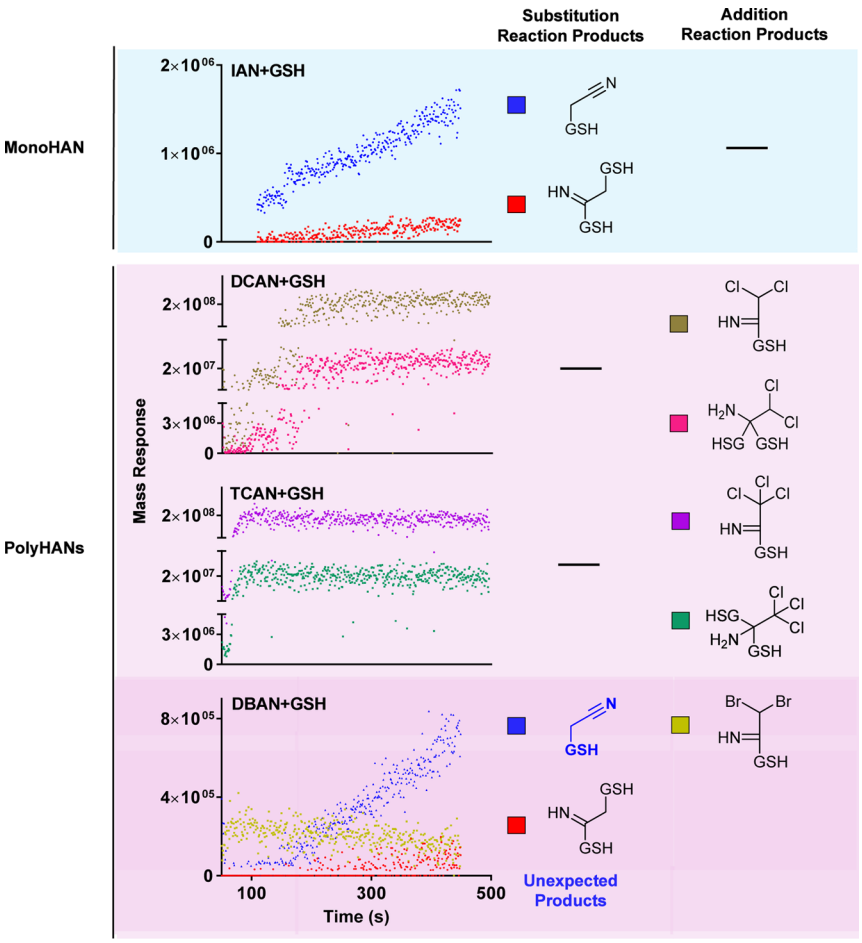

Figure 3. Direct infusion MS analysis of HAN-GSH reaction products. IAN, BAN, CAN, and DBAN (10 μM) were reacted with GSH (1 mM) while DCAN and TCAN (1 mM) were reacted with GSH (1 mM). All products are color coded in the legend on the right.

and Br-analogues. This reactivity trend observed for monoHANs supports our hypothesis that reaction with proteome thiols via S_N2 is likely the major mechanism of toxicity for monoHANs.

We then moved forward to determine the structure-related proteome thiol reactivity of polyHANs. DCAN exhibited little reactivity with proteome thiols which was consistent with its absent bioassay responses. Surprisingly, substantial protein thiol reactivity was observed for TCAN at concentrations (50 μM) akin to monoHANs (Figure 2b), despite its subdued in vitro toxicity in the Nrf2 bioassay. This is interesting as increased thiol ABPP reactivity has been linked to greater Nrf2 responses for similar DBPs like monohaloacetamides and monohaloacetic acids.[29] Like TCAN, DBAN also exhibited strong protein thiol reactivity at 50 μM like those of reactive monoHANs (Figure 2b). Taken together, DBAN's overall cytotoxicity, oxidative stress, and proteome thiol reactivity profiles match the responses of monoHANs better than with other polyHANs. Therefore, given the disagreement between thiol reactivity and in vitro toxicity for polyHANs, their proteome thiol reaction mechanisms appear to be distinct and complicated.

Distinct Reaction Mechanisms Between HANs and Thiols

To elucidate the reaction mechanisms between HANs and thiols, we employed direct infusion high-resolution mass spectrometry. GSH, a widely accepted protein thiol surrogate,[27,57,58] was used to probe the reaction mechanisms. Under pseudo first order conditions (HAN/GSH, 10:1000 μM), both IAN and BAN generated multiple products, while CAN exhibited negligible reactivity (Figures 3 and S1). By using nontargeted analysis, monoHAN-GSH ($C_{12}H_{18}N_4O_6S$, m/z 347.1025, −0.4 ppm) was detected as the primary reaction product. MS^2 spectra confirmed GSH adduction to monoHANs through its thiol moiety (Figure S2), evidencing the canonical S_N2 reaction between thiols and monoHANs. The reactivity trend of IAN > BAN ≫ CAN is expected for S_N2 reactions as S_N2 reactions are governed by leaving group ability. A minor product was assigned as monoHAN-2GSH ($C_{22}H_{35}N_7O_{12}S_2$, m/z 654.1803, 0.8 ppm) with two GSH attached, one through substitution and the other via addition at the nitrile carbon (Figure S3). Collectively, monoHAN was found to react with GSH primarily through the S_N2 reaction, with strong reactivities observed for IAN and BAN. This observation agrees with the bioassay and ABPP results, supporting thiol reactivity by S_N2 as the major mechanism of toxicity for monoHANs.

Our group has previously observed the addition reaction for DCAN with thiols,[27] which was confirmed in this study alongside the TCAN-GSH addition product which was assigned as $C_{12}H_{17}Cl_3N_4O_6S$ (m/z 451.0005, −0.4 ppm) (Figure S4). A previous study also found that TCAN can react with GSH at the nitrile carbon[59] to form the same product we observed at m/z 421.0005. Unlike monoHANs, both polychlorinated HANs reacted with GSH extremely quickly;

https://doi.org/10.1021/acsenvironau.4c00068
ACS Environ. Au 2025, 5, 101−113

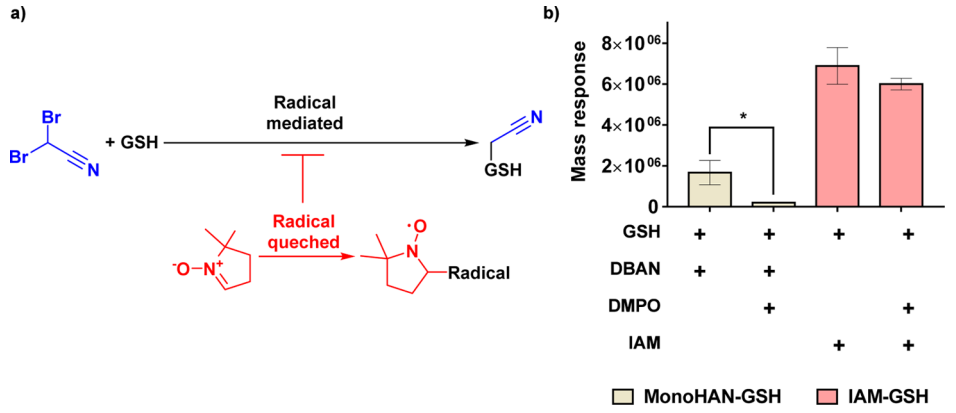

Figure 4. DMPO quenches DBAN-GSH product formation. (a) Reaction scheme between DBAN, GSH, and DMPO. (b) LC−MS intensities of DBAN-GSH with DMPO reaction products. Significant decrease of DBAN-GSH product was observed when DMPO (100 mM) was added to the reaction mixture (n = 3). IAM-GSH positive control mass responses are unaffected by DMPO.

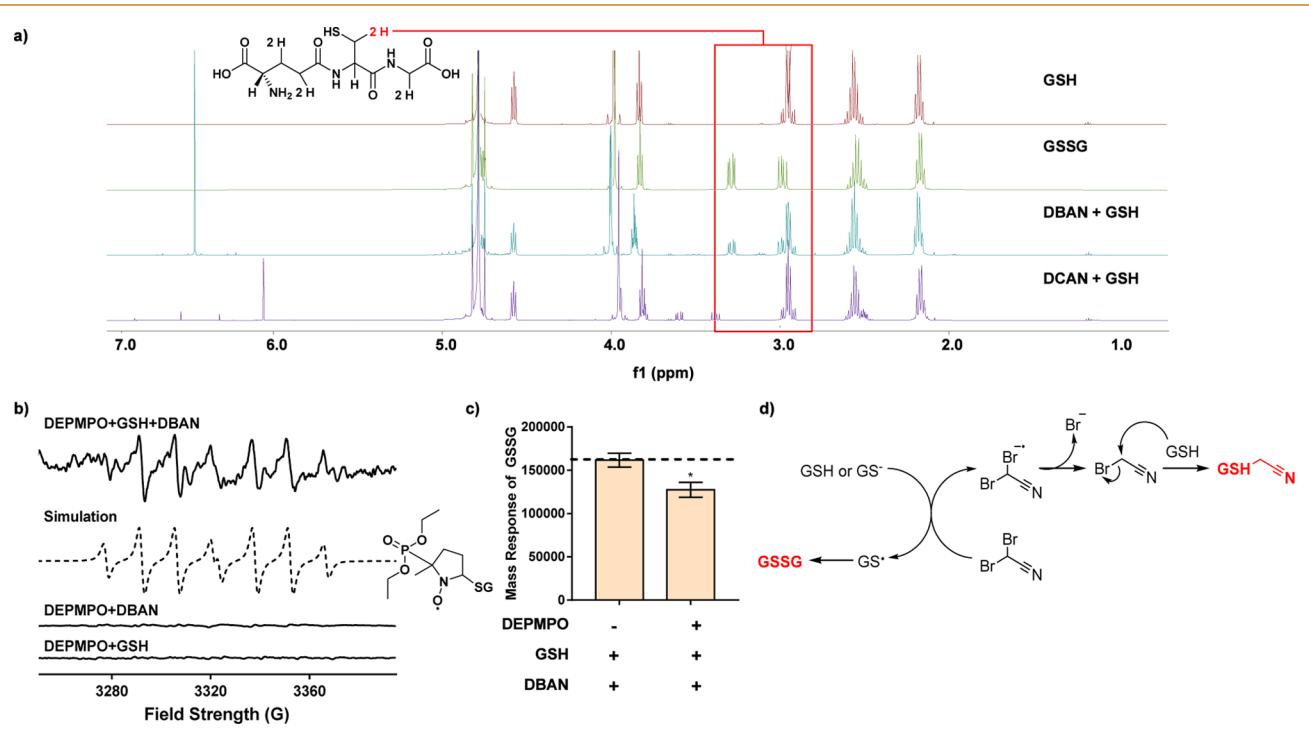

Figure 5. NMR, EPR, and LC−MS reveal a new radical mediated reaction between DBAN and GSH. (a) Proton NMR after a 3 h reaction for (top to bottom): GSH (50 mM); GSSG (50 mM); DBAN (50 mM) and GSH (50 mM); and DCAN (50 mM) and GSH (50 mM). (b) EPR spectra of DEPMPO trapped radical in DBAN-GSH reactions (top), simulated spectra of DEPMPO-SG radical (dashed), and experimental controls (bottom two). (c) LC−MS GSSG detection over various reaction parameters (t = 3 h), asterisks denote p = 0.007. The hyperfine splitting constants for DEPMPO/$^{\bullet}$SG radical are as follows: α^{N} = 14.28 G, α^{P} = 45.80 G, and α^{H} = 14.63 G. (d) Proposed mechanism for the generation of GSSG and debrominated product through reactions between GSH and DBAN.

therefore, to investigate their reaction products, reaction kinetics were slowed by increasing the ratio of HAN/GSH from 0.01 mM:1 mM to 1 mM:1 mM. The products reached steady state at 162 s for DCAN and 44 s for TCAN. The quicker reaction by TCAN can be explained by the increased electronegativity from three chlorines attached at one carbon end which induces a greater partial positive charge at the nitrile carbon. However, TCAN's strong thiol reactivity seems inconsistent with its low Nrf2 bioassay toxicity which is governed by thiol reactivity. A previous study has reported that highly reactive chemicals (i.e., quinones) may present low cellular toxicities due to their sequestration by protein thiols in cell media before penetrating into cells.[60,61] Bovine serum albumin (BSA) is reported to be a sink for reactive chemicals, lowering their apparent cellular concentrations through adduction.[61] Consistent with our observations, TCAN may have been detoxified by its ultrafast, nonreversible reactions with media proteins like BSA at its free thiol residue. This contrasts with monoHANs which react at slower kinetics which may allow cell penetration to be a competitive process against thiol media protein sequestration.

Like its polyhalogenated counterparts, an addition product assigned as $C_{12}H_{18}Br_2N_4O_6S$ (m/z 504.9392, −0.9 ppm) was found for DBAN albeit at low intensities. Unexpectedly, DBAN's primary reaction product was assigned as $C_{12}H_{18}N_4O_6S$ (m/z 347.1015, −1.1 ppm), which is a fully

https://doi.org/10.1021/acsenvironau.4c00068
ACS Environ. Au 2025, 5, 101−113

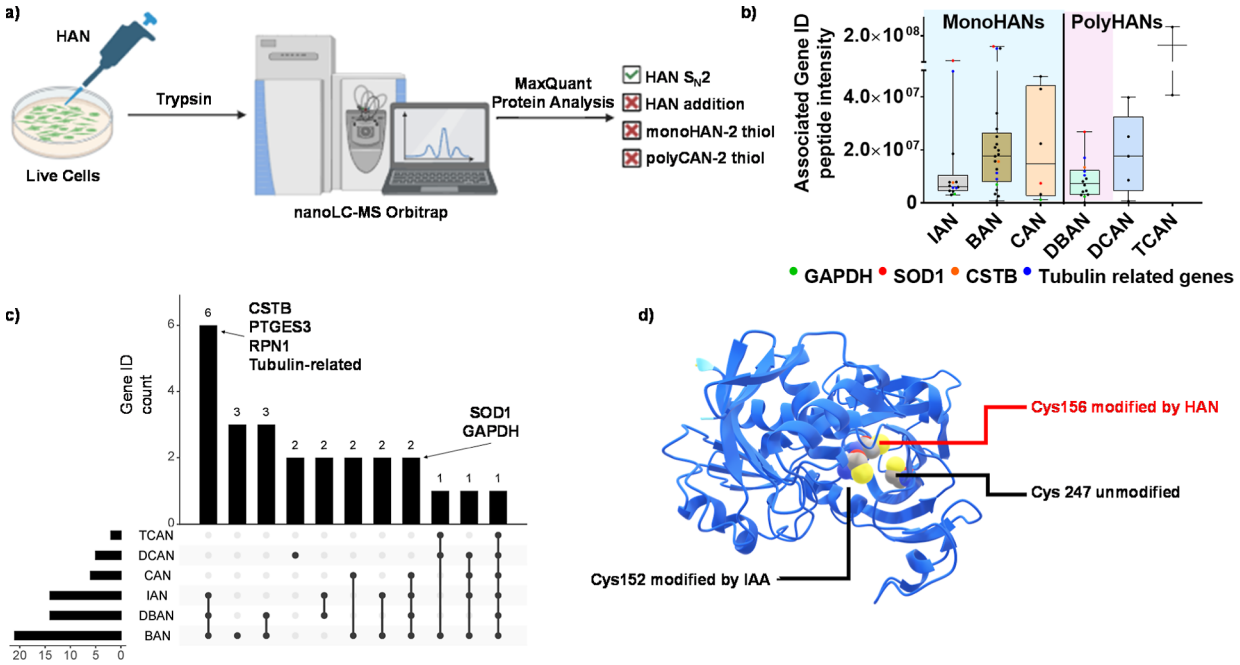

Figure 6. HANs adduct proteins in live cells as revealed by shotgun proteomics. (a) Four types of modifications incorporated for shotgun proteomics. (b) Box and whisker plot of associated gene IDs from monoHAN-S_N2 adducted corresponding peptides. All peptide intensities were normalized to the blank control or 10^4 minimum intensity cutoff. (c) UpSet plot of associated gene IDs identified from in vitro exposure of selected HANs to live cells. (d) AlphaFold representation of GAPDH with Cys 156, Cys 247, and Cys 152 highlighted to have different reported modifications.

debrominated product analogous to the monoHAN-GSH product. Due to the 2 Br on DBAN, it is unlikely that this product was generated via the same S_N2 reaction pathway as monoHANs. To confirm the unexpected reaction, GC−MS was used to quantify DBAN over a reaction period of 72 h with GSH. We observed >50% consumption (p = 0.001) of DBAN (Figure S5) through this reaction. Indeed, a study published 35 years ago by Lin et al., also noticed the formation of the debrominated product of DBAN[59] which cross-validated our results. This debrominated product was unique to DBAN within the polyHAN class. The formation of this unexpected product may partially explain DBAN's unique cytotoxicity and Nrf2 responses compared to the two other polyHANs.

Unique Radical Reactions Regulate the Production of DBAN-Thiol Products

Single electron transfer (SET) has been well documented to facilitate reductive dehalogenation in the presence of reductants.[62,63] Additionally, thiolates are known to assist SET as an electron donor by forming thiyl radicals.[64,65] Combining these two processes, we sought to determine if the DBAN-GSH reaction was radical-mediated. To test this hypothesis, we employed a well studied trapping agent, DMPO, that can adduct a diverse spectrum of radicals (Figure 4a).[66−69] Following a 3 h reaction, DMPO significantly decreased the yield of m/z 347.1015 by >8.4 folds (p = 0.05) relative to the controls in the absence of DMPO (Figure 4b). The same trend was not found for our control compound, IAM (p = 0.2), which reacts with GSH via S_N2 without radical involvement.[27,29,70,71] Furthermore, using nontarget MS, we determined that DMPO does not react with either GSH or DBAN respectively (Figure S6). The DMPO trapping experiment strongly indicates that reactive radical intermediates are directly involved in the DBAN-GSH reaction to form m/z 347.1015. Despite our best efforts to directly monitor the radical species involved using EPR spectroscopy, we did not observe any DMPO trapped radical signals. As the lifetime of DMPO trapped radicals varies from the order of μs to minutes,[67,72,73] the DMPO trapped radical in DBAN-GSH may be extremely short-lived and be below the LOD of the EPR.

We moved onto NMR spectroscopy to further confirm the reaction products between DBAN and GSH. An unexpectedly large signature of glutathione disulfide (GSSG) was detected in DBAN-GSH reaction mixtures and confirmed by authentic standards (Figure 5a). No formation of GSSG was observed for DCAN under the same reaction conditions in NMR. This result was additionally confirmed with direct infusion mass spectrometry which visualized the increase of GSSG ($C_{20}H_{32}N_6O_{12}S_2$, m/z 613.1593, 0.1 ppm) in DBAN-GSH reactions (Figure S7). GSSG is formed when two GSH are oxidized and the ratio between the two species is often indicative of oxidative stress within cells.[74] Therefore, the discovery of the GSSG reaction product in DBAN-GSH reactions further reveals DBAN's unique thiol reactivity compared to other HANs.

Disulfides have been documented to be formed when 2 thiyl radicals terminate.[75−78] Spurred on by our radical results, we decided to use another trapping agent, 5-(diethoxyphosphoryl)-5-methyl-1-pyrroline-*N*-oxide (DEPMPO), which has been reported to generate a more stable trap for thiyl radicals compared to DMPO.[79,80] After incubation of DEPMPO with DBAN and GSH, we captured a 7-line peak radical signal that was specific to the reaction (Figure 5b). To determine the radical species, we used optimized spin fitting parameters in WinSim to produce simulations of O and S radical centered DEPMPO traps (Figure S8). We found that the following hyperfine splitting constants for S radical simulation matched closely with our experimental data: α^N = 14.28 G, α^P = 45.80 G, and α^H = 14.63 G. Moreover, the α^P value is characteristic

https://doi.org/10.1021/acsenvironau.4c00068
ACS Environ. Au 2025, 5, 101−113

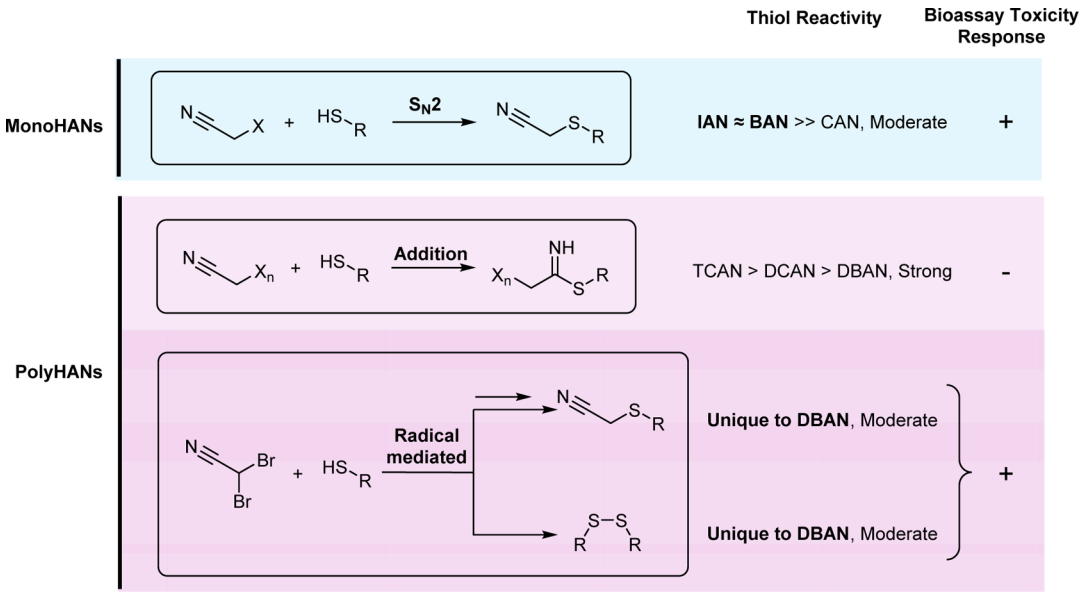

Figure 7. Summary schematic of structure-related toxicity and thiol reactivities of HAN. MonoHANs react solely via S_N2 reaction; polyHANs react through addition which is ultrafast and sequestered by media proteins, resulting in low bioassay assay responses. DBAN reacts through radical pathways leading to debrominated products and GSSG, which causes its unique toxicity which is similar to IAN and BAN.

for thiyl radicals trapped by DEPMPO.[79] Additionally, LC–MS results revealed significant decreases ($p = 0.007$) of GSSG after addition of DEPMPO in DBAN-GSH reactions compared to native reaction conditions (Figure 5c) which further confirm that GSSG is formed through thiyl radicals mechanisms. Like DMPO, DEPMPO was not found to react with either of the reagents (Figure S9). DEPMPO was able to trap thiyl radicals only when both DBAN and GSH were present. Together, we propose that DBAN reacts with GSH by undergoing SET and generating GS-radicals which combine to form GSSG (Figure 5d). After SET, the resulting DBAN radical is unstable and will likely undergo mesolytic cleavage to form a carbon radical which can abstract a hydrogen, thus forming BAN. The debromination pathway is well documented for bromine chemicals undergoing SET.[81−83] The resulting BAN from the radical mediated debromination of DBAN will undergo typical monoHAN-thiol S_N2 reactions to form m/z 347.1015 (Figure 5d). This is supported by the similar kinetics for the formation of the m/z 347.1015 product in monoHAN and DBAN-thiol reactions.

Shotgun Proteomics Confirmed the Adduction of Proteome by HAN in Live MCF7 Cells

To further confirm if the observed acellular reactions could be replicated at physiologically relevant conditions, shotgun proteomics was used to monitor HAN protein adducts in live, adherent MCF7 cells exposed to HANs (Figure 6a). Using the HAN-thiol reactions discussed above, the anticipated protein adduct modifications were searched across samples. Out of the 4 modification types, only the monoHAN-GSH adduct signature (C_2H_2N) was detected (Figure 6b). In total, 58 peptides across all tested HANs were identified to have protein adducts. The HAN with the most adducts was BAN which adducted to 21 peptides, followed by IAN with 14 adducted peptides. In contrast, CAN only adducted to 4 peptides. Collectively, the in vitro proteomics for monoHANs mirror their S_N2 reactivity trends and toxicities. Only a small number of adducted peptides were detected for TCAN (2) and DCAN (5), consistent with their low Nrf2 bioassay responses.

Unlike the other polyHANs, 14 peptide adducts were observed for DBAN. Of these, 6 peptides were common with IAN and BAN which was the highest degree of similarity found among all tested HANs (Figure 6c). This observation reinforces the similarities found in DBAN and monoHAN bioassay profiles, thiol reactivity, and common GSH products. Within these 6 common adducted peptides, half are associated with antioxidant signaling and are ROS targets,[84−86] including glyceraldehyde 3-phosphate dehydrogenase (GAPDH), cystatin B (CSTB), and superoxide dismutase 1 (SOD1). SOD1 was adducted most by BAN ($5.90 \times 10^7 \pm 2.12 \times 10^7$ peptide intensity), IAN ($1.39 \times 10^8 \pm 4.45 \times 10^7$ peptide intensity), and DBAN ($2.68 \times 10^7 \pm 1.65 \times 10^7$ peptide intensity). All HANs adducted to SOD1 at Cys 111. This observation is aligned with a previous study that found SOD1 modification at Cys 111 by IAM.[87] This demonstrated that HANs and DBPs selectively attack hypersensitive cysteine residues. Modifications at Cys 111 are known to cause misfolding and protein aggregation[88] and previous studies have found reduced SOD1 activity in murine stomachs after DBAN exposure.[89] GAPDH was found to be preferentially modified at Cys 156 by both monoHANs and DBAN (Figures 6d and S10). This is surprising as Cys156 is a buried cysteine and previous studies have discovered that another DBP, iodoacetic acid (IAA), selectively adducts to the more available Cys 152 site instead.[29] This demonstrates that distinct proteome cysteine reactivities depend on DBP chemical structures, which may lead to complicated and distinct toxicity pathways. Collectively, the proteomics profile supported the formation of debrominated protein adducts from DBAN and S_N2 adducts from monoHANs in live cells, supporting that the proposed radical and S_N2 reactions are also physiologically relevant.

Implications

We herein demonstrated that the cellular toxicities of HANs are determined by their distinct structure-related thiol reaction pathways (Figure 7). MonoHAN toxicity is governed through

https://doi.org/10.1021/acsenvironau.4c00068
ACS Environ. Au 2025, 5, 101−113

S_N2-leaving group trends much like other monohalogenated DBPs.[27,29] Although DBAN and monoHANs share many similarities, DBAN's radical-mediated formation of debrominated products is unique. To the best of our knowledge, DBAN's unique ability to generate GSSG and its debrominated product through radical reactions has not been reported before. These novel products offer insight into the enhanced toxicity of DBAN in vitro, relative to other HANs. This unique chemical behavior necessitates further exploration to determine whether similar reaction mechanisms are applicable to other dibrominated DBPs.

In this study, we only observed toxicity for HANs that were able to generate dehalogenated products. TCAN and DCAN showed little cellular toxicity despite their significant reactivity with thiols. Both partitioning and reactivity might influence the cellular concentrations of chemicals and hence their apparent toxicity.[61] The log *P* values of TCAN (1.28)[90] and DCAN (0.88)[91] are similar to those of DBAN (1.29)[92] and monoHANs (0.33−0.93).[93−95] Thus, partitioning should not explain the 10−100 times lower toxicity of TCAN and DCAN. Instead, this is more likely attributed to their ultrafast addition reactions with media proteins that can lead to the nonreversible sequestration of TCAN and DCAN in cell culture media preventing cell penetration. However, TCAN and DCAN may be toxic in vivo where free thiols are not present at high concentrations to sequester polyHANs. Therefore, in vivo studies are warranted to determine if the ultrafast polyHAN addition reactions are physiologically relevant and/or toxic in the future.

■ ASSOCIATED CONTENT

Supporting Information

The Supporting Information is available free of charge at https://pubs.acs.org/doi/10.1021/acsenvironau.4c00068.

The Supporting Information provides text and figures addressing: (1) GC−MS methodology, (2) BAN and CAN reaction products with GSH, (3) MonoHAN-GSH MS^2 spectrum, (4) MonoHAN-2GSH MS^2 spectrum, (5) PolyHAN-GSH addition product full MS spectrum, (6) DBAN GC−MS calibration curve and DBAN-GSH reaction monitoring >72 h, (7) DMPO-GSH and DMPO−DBAN reaction mixture nontarget analyses, (8) direct infusion data for all DBAN-GSH products, (9) EPR spectra of the DEPMPO-GSH-DBAN reaction with S and O-centered radical simulation spectra, (10) DEPMPO-GSH and DEPMPO−DBAN reaction mixture nontarget analyses, and (11) representative MS^2 spectrum of an HAN adducted peptide (PDF)

■ AUTHOR INFORMATION

Corresponding Author

Hui Peng − *Department of Chemistry, University of Toronto, Toronto, Ontario M5S 3H6, Canada; School of the Environment, University of Toronto, Toronto, Ontario M5S 3J1, Canada;* orcid.org/0000-0002-2777-0588; Email: hui.peng@utoronto.ca

Authors

Kirsten Yeung − *Department of Chemistry, University of Toronto, Toronto, Ontario M5S 3H6, Canada; School of the Environment, University of Toronto, Toronto, Ontario M5S 3J1, Canada*

Linna Xie − *Department of Chemistry, University of Toronto, Toronto, Ontario M5S 3H6, Canada*

Pranav Nair − *Department of Chemistry, University of Toronto, Toronto, Ontario M5S 3H6, Canada*

Complete contact information is available at: https://pubs.acs.org/10.1021/acsenvironau.4c00068

Notes

The authors declare no competing financial interest.

■ ACKNOWLEDGMENTS

This research was supported by the National Sciences and Engineering Research Council (NSERC) CRD and Discovery grants. The authors acknowledge the support of instrumentation grants from the Canada Foundation for Innovation, the Ontario Research Fund, the NSERC Research Tools and Instrument Grant. The authors thank the support of the Miriam Diamond group at the University of Toronto, and particularly Sara Vaezafshar, for their generous help with their gas chromatography mass spectrometer.

■ REFERENCES

(1) Shi, J.; Zhang, K.; Xiao, T.; Yang, J.; Sun, Y.; Yang, C.; Dai, H.; Yang, W. Exposure to Disinfection By-Products and Risk of Cancer: A Systematic Review and Dose-Response Meta-Analysis. *Ecotoxicol. Environ. Saf.* **2024**, *270*, 115925.

(2) Villanueva, C. M.; Cantor, K. P.; Grimalt, J. O.; Malats, N.; Silverman, D.; Tardon, A.; Garcia-Closas, R.; Serra, C.; Carrato, A.; Castaño-Vinyals, G.; Marcos, R.; Rothman, N.; Real, F. X.; Dosemeci, M.; Kogevinas, M. Bladder Cancer and Exposure to Water Disinfection By-Products through Ingestion, Bathing, Showering, and Swimming in Pools. *Am. J. Epidemiol.* **2006**, *165* (2), 148−156.

(3) Evlampidou, I.; Font-Ribera, L.; Rojas-Rueda, D.; Gracia-Lavedan, E.; Costet, N.; Pearce, N.; Vineis, P.; Jaakkola, J. J. K.; Delloye, F.; Makris, K. C.; Stephanou, E. G.; Kargaki, S.; Kozisek, F.; Sigsgaard, T.; Hansen, B.; Schullehner, J.; Nahkur, R.; Galey, C.; Zwiener, C.; Vargha, M.; Righi, E.; Aggazzotti, G.; Kalnina, G.; Grazuleviciene, R.; Polanska, K.; Gubkova, D.; Bitenc, K.; Goslan, E. H.; Kogevinas, M.; Villanueva, C. M. Trihalomethanes in Drinking Water and Bladder Cancer Burden in the European Union. *Environ. Health Perspect.* **2020**, *128* (1), 17001.

(4) Weisman, R. J.; Heinrich, A.; Letkiewicz, F.; Messner, M.; Studer, K.; Wang, L.; Regli, S. Estimating National Exposures and Potential Bladder Cancer Cases Associated with Chlorination DBPs in U.S. Drinking Water. *Environ. Health Perspect.* **2022**, *130* (8), 87002.

(5) Richardson, S. D. Tackling Unknown Disinfection By-Products: Lessons Learned. *J. Hazard. Mater. Lett.* **2021**, *2*, 100041.

(6) Richardson, S. D.; Plewa, M. J.; Wagner, E. D.; Schoeny, R.; DeMarini, D. M. Occurrence, Genotoxicity, and Carcinogenicity of Regulated and Emerging Disinfection by-Products in Drinking Water: A Review and Roadmap for Research. *Mutat. Res.* **2007**, *636* (1−3), 178−242.

(7) Li, X. F.; Mitch, W. A. Drinking Water Disinfection Byproducts (DBPs) and Human Health Effects: Multidisciplinary Challenges and Opportunities. *Environ. Sci. Technol.* **2018**, *52* (4), 1681−1689.

(8) Guidelines for Canadian Drinking Water Quality: Guideline Technical Document—Haloacetic Acids—Canada.ca. https://www.canada.ca/en/health-canada/services/publications/healthy-living/guidelines-canadian-drinking-water-quality-guideline-technical-document-haloacetic-acids.html (accessed Apr 9, 2024).

(9) Guidelines for Canadian Drinking Water Quality: Guideline Technical Document—Trihalomethanes—Canada.ca. https://www.canada.ca/en/health-canada/services/publications/healthy-living/guidelines-canadian-drinking-water-quality-trihalomethanes.html (accessed Apr 9, 2024).

(10) Richardson, S. D.; Plewa, M. J. To Regulate or Not to Regulate? What to Do with More Toxic Disinfection by-Products? *J. Environ. Chem. Eng.* **2020**, *8* (4), 103939.
(11) McKenna, E.; Thompson, K. A.; Taylor-Edmonds, L.; McCurry, D. L.; Hanigan, D. Summation of Disinfection By-Product CHO Cell Relative Toxicity Indices: Sampling Bias, Uncertainty, and a Path Forward. *Environ. Sci.:Processes Impacts* **2020**, *22* (3), 708−718.
(12) Stewart, K.; An, D.; Hanigan, D. Reduction of Haloacetonitrile-Associated Risk by Adjustment of Distribution System PH. *Environ. Sci.:Water Res. Technol.* **2023**, *9* (10), 2725−2732.
(13) Huang, H.; Wu, Q. Y.; Hu, H. Y.; Mitch, W. A. Dichloroacetonitrile and Dichloroacetamide Can Form Independently during Chlorination and Chloramination of Drinking Waters, Model Organic Matters, and Wastewater Effluents. *Environ. Sci. Technol.* **2012**, *46* (19), 10624−10631.
(14) Zeng, T.; Plewa, M. J.; Mitch, W. A. N-Nitrosamines and Halogenated Disinfection Byproducts in U.S. Full Advanced Treatment Trains for Potable Reuse. *Water Res.* **2016**, *101*, 176−186.
(15) Krasner, S. W.; Weinberg, H. S.; Richardson, S. D.; Pastor, S. J.; Chinn, R.; Sclimenti, M. J.; Onstad, G. D.; Thruston, A. D. Occurrence of a New Generation of Disinfection Byproducts. *Environ. Sci. Technol.* **2006**, *40* (23), 7175−7185.
(16) Chuang, Y. H.; Tung, H. H. Formation of Trichloronitromethane and Dichloroacetonitrile in Natural Waters: Precursor Characterization, Kinetics and Interpretation. *J. Hazard. Mater.* **2015**, *283*, 218−226.
(17) Muellner, M. G.; Wagner, E. D.; Mccalla, K.; Richardson, S. D.; Woo, Y. T.; Plewa, M. J. Haloacetonitriles vs. Regulated Haloacetic Acids: Are Nitrogen-Containing DBFs More Toxic? *Environ. Sci. Technol.* **2007**, *41* (2), 645−651.
(18) Richardson, S. D.; Thruston, A. D.; Krasner, S. W.; Weinberg, H. S.; Miltner, R. J.; Schenck, K. M.; Narotsky, M. G.; McKague, A. B.; Simmons, J. E. Integrated Disinfection By-Products Mixtures Research: Comprehensive Characterization of Water Concentrates Prepared from Chlorinated and Ozonated/Postchlorinated Drinking Water. *J. Toxicol. Environ. Health, Part A* **2008**, *71* (17), 1165−1186.
(19) Wei, X.; Yang, M.; Zhu, Q.; Wagner, E. D.; Plewa, M. J. Comparative Quantitative Toxicology and QSAR Modeling of the Haloacetonitriles: Forcing Agents of Water Disinfection Byproduct Toxicity. *Environ. Sci. Technol.* **2020**, *54* (14), 8909−8918.
(20) Federal Register Drinking Water Contaminant Candidate List 5-Final. https://www.federalregister.gov/documents/2022/11/14/2022-23963/drinking-water-contaminant-candidate-list-5-final (accessed Apr 5, 2024).
(21) Ahmed, A. E.; Hussein, G. I.; Loh, J.-P.; Abdel-Rahman, S. Z. Studies on the Mechanism of Haloacetonitrile-Induced Gastrointestinal Toxicity: Interaction of Dibromoacetonitrile with Glutathione and Glutathione-S-Transferase in Rats. *J. Biochem. Toxicol.* **1991**, *6* (2), 115−121.
(22) Lipscomb, J. C.; El-Demerdash, E.; Ahmed, A. E. Haloacetonitriles: Metabolism and Toxicity. *Rev. Environ. Contam. Toxicol.* **2009**, *198*, 169−200.
(23) Ahmed, A. E.; Soliman, S. A.; Loh, J. P.; Hussein, G. I. Studies on the Mechanism of Haloacetonitriles Toxicity: Inhibition of Rat Hepatic Glutathione S-Transferases In Vitro. *Toxicol. Appl. Pharmacol.* **1989**, *100* (2), 271−279.
(24) Lin, E. L. C.; Daniel, F. B.; Herren-Freund, S. L.; Pereira, M. A. Haloacetonitriles: Metabolism, Genotoxicity, and Tumor-Initiating Activity. *Environ. Health Perspect.* **1986**, *69*, 67.
(25) Zhang, S. H.; Miao, D. Y.; Tan, L.; Liu, A. L.; Lu, W. Q. Comparative Cytotoxic and Genotoxic Potential of 13 Drinking Water Disinfection By-Products Using a Microplate-Based Cytotoxicity Assay and a Developed SOS/Umu Assay. *Mutagenesis* **2015**, *31* (1), 35−41.
(26) Dong, S.; Page, M. A.; Wagner, E. D.; Plewa, M. J. Thiol Reactivity Analyses to Predict Mammalian Cell Cytotoxicity of Water Samples. *Environ. Sci. Technol.* **2018**, *52* (15), 8822−8829.
(27) Yeung, K.; Moore, N.; Sun, J.; Taylor-Edmonds, L.; Andrews, S.; Hofmann, R.; Peng, H. Thiol Reactome: A Nontargeted Strategy to Precisely Identify Thiol Reactive Drinking Water Disinfection Byproducts. *Environ. Sci. Technol.* **2023**, *57* (47), 18722−18734.
(28) Pals, J. A.; Ang, J. K.; Wagner, E. D.; Plewa, M. J. Biological Mechanism for the Toxicity of Haloacetic Acid Drinking Water Disinfection Byproducts. *Environ. Sci. Technol.* **2011**, *45* (13), 5791−5797.
(29) Hall, D. R.; Yeung, K.; Peng, H. Monohaloacetic Acids and Monohaloacetamides Attack Distinct Cellular Proteome Thiols. *Environ. Sci. Technol.* **2020**, *54* (23), 15191−15201.
(30) Pals, J. A.; Wagner, E. D.; Plewa, M. J. Energy of the Lowest Unoccupied Molecular Orbital, Thiol Reactivity, and Toxicity of Three Monobrominated Water Disinfection Byproducts. *Environ. Sci. Technol.* **2016**, *50* (6), 3215−3221.
(31) Escher, B. I.; Dutt, M.; Maylin, E.; Tang, J. Y. M.; Toze, S.; Wolf, C. R.; Lang, M. Water Quality Assessment Using the AREc32 Reporter Gene Assay Indicative of the Oxidative Stress Response Pathway. *J. Environ. Monit.* **2012**, *14* (11), 2877−2885.
(32) Stalter, D.; O'Malley, E.; Von Gunten, U.; Escher, B. I. Fingerprinting the Reactive Toxicity Pathways of 50 Drinking Water Disinfection By-Products. *Water Res.* **2016**, *91*, 19−30.
(33) Wang, S.; Zheng, W.; Liu, X.; Xue, P.; Jiang, S.; Lu, D.; Zhang, Q.; He, G.; Pi, J.; Andersen, M. E.; Tan, H.; Qu, W. Iodoacetic Acid Activates Nrf2-Mediated Antioxidant Response In Vitro and In Vivo. *Environ. Sci. Technol.* **2014**, *48* (22), 13478−13488.
(34) Pals, J.; Attene-Ramos, M. S.; Xia, M.; Wagner, E. D.; Plewa, M. J. Human Cell Toxicogenomic Analysis Linking Reactive Oxygen Species to the Toxicity of Monohaloacetic Acid Drinking Water Disinfection Byproducts. *Environ. Sci. Technol.* **2013**, *47* (21), 12514−12523.
(35) Sun, J.; Peng, H.; Alharbi, H. A.; Jones, P. D.; Giesy, J. P.; Wiseman, S. B. Identification of Chemicals that Cause Oxidative Stress in Oil Sands Process-Affected Water. *Environ. Sci. Technol.* **2017**, *51* (15), 8773−8781.
(36) Jeong, C. H.; Wagner, E. D.; Siebert, V. R.; Anduri, S.; Richardson, S. D.; Daiber, E. J.; McKague, A. B.; Kogevinas, M.; Villanueva, C. M.; Goslan, E. H.; Luo, W.; Isabelle, L. M.; Pankow, J. F.; Grazuleviciene, R.; Cordier, S.; Edwards, S. C.; Righi, E.; Nieuwenhuijsen, M. J.; Plewa, M. J. Occurrence and Toxicity of Disinfection Byproducts in European Drinking Waters in Relation with the HIWATE Epidemiology Study. *Environ. Sci. Technol.* **2012**, *46* (21), 12120−12128.
(37) Zhang, Y.; Han, X.; Niu, Z. Health Risk Assessment of Haloacetonitriles in Drinking Water Based on Internal Dose. *Environ. Pollut.* **2018**, *236*, 899−906.
(38) Escher, B. I.; Blanco, J.; Caixach, J.; Cserbik, D.; Farré, M. J.; Flores, C.; König, M.; Lee, J.; Nyffeler, J.; Planas, C.; Redondo-Hasselerharm, P. E.; Rovira, J.; Sanchís, J.; Schuhmacher, M.; Villanueva, C. M. In Vitro Bioassays for Monitoring Drinking Water Quality of Tap Water, Domestic Filtration and Bottled Water. *J. Expo. Sci. Environ. Epidemiol.* **2023**, *34* (1), 126−135.
(39) Han, J.; Wang, S.; Yeung, K.; Yang, D.; Gu, W.; Ma, Z.; Sun, J.; Wang, X.; Chow, C. W.; Chan, A. W. H.; Peng, H. Proteome-Wide Effects of Naphthalene-Derived Secondary Organic Aerosol in BEAS-2B Cells Are Caused by Short-Lived Unsaturated Carbonyls. *Proc. Natl. Acad. Sci. U.S.A.* **2020**, *117* (41), 25386−25395.
(40) Cravatt, B. F.; Wright, A. T.; Kozarich, J. W. Activity-Based Protein Profiling: From Enzyme Chemistry to Proteomic Chemistry. *Annu. Rev. Biochem.* **2008**, *77* (77), 383−414.
(41) Leavens, T. L.; Blount, B. C.; Demarini, D. M.; Madden, M. C.; Valentine, J. L.; Case, M. W.; Silva, L. K.; Warren, S. H.; Hanley, N. M.; Pegram, R. A. Disposition of Bromodichloromethane in Humans Following Oral and Dermal Exposure. *Toxicol. Sci.* **2007**, *99* (2), 432−445.
(42) Rivera-Núñez, Z.; Wright, J. M.; Blount, B. C.; Silva, L. K.; Jones, E.; Chan, R. L.; Pegram, R. A.; Singer, P. C.; Savitz, D. A. Comparison of Trihalomethanes in Tap Water and Blood: A Case Study in the United States. *Environ. Health Perspect.* **2012**, *120* (5), 661−667.

(43) Ashley, D. L.; Blount, B. C.; Singer, P. C.; Depaz, E.; Wilkes, C.; Gordon, S.; Lyu, C.; Masters, J. Changes in Blood Trihalomethane Concentrations Resulting from Differences in Water Quality and Water Use Activities. *Arch. Environ. Occup. Health* **2005**, *60* (1), 7−15.
(44) Homer, N. Z. M.; Reglinski, J.; Sowden, R.; Spickett, C. M.; Wilson, R.; Walker, J. J. Dimethylsulfoxide Oxidizes Glutathione In Vitro and in Human Erythrocytes: Kinetic Analysis by 1H NMR. *Cryobiology* **2005**, *50* (3), 317−324.
(45) Kutarna, S.; Tang, S.; Hu, X.; Peng, H. Enhanced Nontarget Screening Algorithm Reveals Highly Abundant Chlorinated Azo Dye Compounds in House Dust. *Environ. Sci. Technol.* **2021**, *55* (8), 4729−4739.
(46) Smith, C. A.; Want, E. J.; O'Maille, G.; Abagyan, R.; Siuzdak, G. XCMS: Processing Mass Spectrometry Data for Metabolite Profiling Using Nonlinear Peak Alignment, Matching, and Identification. *Anal. Chem.* **2006**, *78* (3), 779−787.
(47) Zhang, H.; Zhang, Y.; Shi, Q.; Zheng, H.; Yang, M. Characterization of Unknown Brominated Disinfection Byproducts during Chlorination Using Ultrahigh Resolution Mass Spectrometry. *Environ. Sci. Technol.* **2014**, *48* (6), 3112−3119.
(48) Peng, H.; Chen, C.; Saunders, D. M. V.; Sun, J.; Tang, S.; Codling, G.; Hecker, M.; Wiseman, S.; Jones, P. D.; Li, A.; Rockne, K. J.; Giesy, J. P. Untargeted Identification of Organo-Bromine Compounds in Lake Sediments by Ultrahigh-Resolution Mass Spectrometry with the Data-Independent Precursor Isolation and Characteristic Fragment Method. *Anal. Chem.* **2015**, *87* (20), 10237−10246.
(49) Schymanski, E. L.; Jeon, J.; Gulde, R.; Fenner, K.; Ruff, M.; Singer, H. P.; Hollender, J. Identifying Small Molecules via High Resolution Mass Spectrometry: Communicating Confidence. *Environ. Sci. Technol.* **2014**, *48* (4), 2097−2098.
(50) Goldman, J. M.; Murr, A. S.; Buckalew, A. R.; Ferrell, J. M.; Cooper, R. L. Moderating Influence of the Drinking Water Disinfection By-Product Dibromoacetic Acid on a Dithiocarbamate-Induced Suppression of the Luteinizing Hormone Surge in Female Rats. *Reprod. Toxicol.* **2007**, *23* (4), 541−549.
(51) Liu, C.; Deng, Y. L.; Yuan, X. Q.; Chen, P. P.; Miao, Y.; Luo, Q.; Zhang, M.; Cui, F. P.; Yao, W.; Zeng, J. Y.; Shi, T.; Lu, T. T.; Li, Y. F.; Lu, W. Q.; Zeng, Q. Exposure to Disinfection By-Products and Reproductive Hormones among Women: Results from the Tongji Reproductive and Environmental (TREE) Study. *Environ. Res.* **2022**, *209*, 112863.
(52) Lou, J.; Wang, W.; Zhu, L. Occurrence, Formation, and Oxidative Stress of Emerging Disinfection Byproducts, Halobenzoquinones, in Tea. *Environ. Sci. Technol.* **2019**, *53* (20), 11860−11868.
(53) Liu, C.; Wang, Y. X.; Chen, Y. J.; Sun, Y.; Huang, L. L.; Cheng, Y. H.; Liu, E. N.; Lu, W. Q.; Messerlian, C. Blood and Urinary Biomarkers of Prenatal Exposure to Disinfection Byproducts and Oxidative Stress: A Repeated Measurement Analysis. *Environ. Int.* **2020**, *137*, 105518.
(54) Brzuzan, P.; Mazur-Marzec, H.; Florczyk, M.; Stefaniak, F.; Fidor, A.; Konkel, R.; Woźny, M. Luciferase Reporter Assay for Small-Molecule Inhibitors of MIR92b-3p Function: Screening Cyanopeptolins Produced by Nostoc from the Baltic Sea. *Toxicol. Vitro* **2020**, *68*, 104951.
(55) Dong, H.; Cuthbertson, A. A.; Plewa, M. J.; Weisbrod, C. R.; McKenna, A. M.; Richardson, S. D. Unravelling High-Molecular-Weight DBP Toxicity Drivers in Chlorinated and Chloraminated Drinking Water: Effect-Directed Analysis of Molecular Weight Fractions. *Environ. Sci. Technol.* **2023**, *57* (47), 18788−18800.
(56) Hu, S.; Li, X.; Gong, T.; Tian, G.; Guo, S.; Huo, C.; Wan, J.; Liu, R. New Mechanistic Insights into Halogen-Dependent Cytotoxic Pattern of Monohaloacetamide Disinfection Byproducts. *J. Hazard. Mater.* **2024**, *465*, 133132.
(57) Böhme, A.; Thaens, D.; Paschke, A.; Schüürmann, G. Kinetic Glutathione Chemoassay to Quantify Thiol Reactivity of Organic Electrophiles—Application to α,β-Unsaturated Ketones, Acrylates, and Propiolates. *Chem. Res. Toxicol.* **2009**, *22* (4), 742−750.
(58) Petri, L.; Ábrányi-Balogh, P.; Varga, P. R.; Imre, T.; Keserű, G. M. Comparative Reactivity Analysis of Small-Molecule Thiol Surrogates. *Bioorg. Med. Chem.* **2020**, *28* (7), 115357.
(59) Lin, E. L. C.; Guion, C. W. Interaction of Haloacetonitriles with Glutathione and Glutathione-S-Transferase. *Biochem. Pharmacol.* **1989**, *38* (4), 685−688.
(60) Wang, X.; Thomas, B.; Sachdeva, R.; Arterburn, L.; Frye, L.; Hatcher, P. G.; Cornwell, D. G.; Ma, J. Mechanism of Arylating Quinone Toxicity Involving Michael Adduct Formation and Induction of Endoplasmic Reticulum Stress. *Proc. Natl. Acad. Sci. U.S.A.* **2006**, *103* (10), 3604−3609.
(61) Proença, S.; Escher, B. I.; Fischer, F. C.; Fisher, C.; Grégoire, S.; Hewitt, N. J.; Nicol, B.; Paini, A.; Kramer, N. I. Effective Exposure of Chemicals in In Vitro Cell Systems: A Review of Chemical Distribution Models. *Toxicol. Vitro* **2021**, *73*, 105133.
(62) Motornov, V. A.; Muzalevskiy, V. M.; Tabolin, A. A.; Novikov, R. A.; Nelyubina, Y. V.; Nenajdenko, V. G.; Ioffe, S. L. Radical Nitration-Debromination of α-Bromo-α-Fluoroalkenes as a Stereoselective Route to Aromatic α-Fluoronitroalkenes—Functionalized Fluorinated Building Blocks for Organic Synthesis. *J. Org. Chem.* **2017**, *82* (10), 5274−5284.
(63) Devery, J. J.; Nguyen, J. D.; Dai, C.; Stephenson, C. R. J. Light-Mediated Reductive Debromination of Unactivated Alkyl and Aryl Bromides. *ACS Catal.* **2016**, *6* (9), 5962−5967.
(64) Andrieux, C. P.; Blocman, C.; Dumas-Bouchiat, J. M.; M'Halla, F.; Savéant, J. M. Determination of the Lifetimes of Unstable Ion Radicals by Homogeneous Redox Catalysis of Electrochemical Reactions. Application to the Reduction of Aromatic Halides. *J. Am. Chem. Soc.* **1980**, *102* (11), 3806−3813.
(65) Wang, S.; Wang, H.; König, B. Light-Induced Single-Electron Transfer Processes Involving Sulfur Anions as Catalysts. *J. Am. Chem. Soc.* **2021**, *143* (38), 15530−15537.
(66) Kalyanaraman, B.; Karoui, H.; Singh, R. J.; Felix, C. C. Detection of Thiyl Radical Adducts Formed during Hydroxyl Radical- and Peroxynitrite-Mediated Oxidation of Thiols—A High Resolution ESR Spin-Trapping Study at Q-Band (35 GHz). *Anal. Biochem.* **1996**, *241* (1), 75−81.
(67) Xie, L. N.; Shao, J.; Huang, C. H.; Li, F.; Xu, D.; Kalyanaraman, B.; Zhu, B. Z. An Unusual Double Radical Homolysis Mechanism for the Unexpected Activation of the Aldoxime Nerve-Agent Antidotes by Polyhalogenated Quinoid Carcinogens under Normal Physiological Conditions. *Free Radic. Biol. Med.* **2019**, *130*, 1−7.
(68) Taniguchi, H.; Madden, K. P. DMPO-Alkyl Radical Spin Trapping: An In Situ Radiolysis Steady-State ESR Study. *Radiat. Res.* **2000**, *153* (4), 447−453.
(69) Mason, R. P. Using Anti-5,5-Dimethyl-1-Pyrroline N-Oxide (Anti-DMPO) to Detect Protein Radicals in Time and Space with Immuno-Spin Trapping. *Free Radic. Biol. Med.* **2004**, *36* (10), 1214−1223.
(70) Murphy, E. R. L.; Joy, A. P.; Ouellette, R. J.; Barnett, D. A. Optimization of Cysteine Residue Alkylation Using an On-Line LC-MS Strategy: Benefits of Using a Cocktail of Haloacetamide Reagents. *Anal. Biochem.* **2021**, *619*, 114137.
(71) Hill, B. G.; Reily, C.; Oh, J.-Y.; Johnson, M. S.; Landar, A. Methods for the Determination and Quantification of the Reactive Thiol Proteome. *Free Radic. Biol. Med.* **2009**, *47*, 675−683.
(72) Zhao, H.; Jiang, J.; Wang, Y.; Lehmler, H. J.; Buettner, G. R.; Quan, X.; Chen, J. Monohydroxylated Polybrominated Diphenyl Ethers (OH-PBDEs) and Dihydroxylated Polybrominated Biphenyls (Di-OH-PBBs): Novel Photoproducts of 2,6-Dibromophenol. *Environ. Sci. Technol.* **2015**, *49* (24), 14120.
(73) Qian, S. Y.; Wang, H. P.; Schafer, F. Q.; Buettner, G. R. EPR Detection of Lipid-Derived Free Radicals from PUFA, LDL, and Cell Oxidations. *Free Radic. Biol. Med.* **2000**, *29* (6), 568−579.
(74) Lahiri, S. S. Fly Ash: Safety and Health Issues. *Handbook of Fly Ash*; Elsevier, 2022, pp 77−224..
(75) Ulrich, K.; Jakob, U. The Role of Thiols in Antioxidant Systems. *Free Radic. Biol. Med.* **2019**, *140*, 14−27.

https://doi.org/10.1021/acsenvironau.4c00068
ACS Environ. Au 2025, 5, 101−113

(76) Valko, M.; Morris, H.; Cronin, M. Metals, Toxicity and Oxidative Stress. *Curr. Med. Chem.* **2005**, *12* (10), 1161−1208.
(77) Jomova, K.; Raptova, R.; Alomar, S. Y.; Alwasel, S. H.; Nepovimova, E.; Kuca, K.; Valko, M. Reactive Oxygen Species, Toxicity, Oxidative Stress, and Antioxidants: Chronic Diseases and Aging. *Arch. Toxicol.* **2023**, *97* (10), 2499−2574.
(78) Kim, H. J.; Ha, S.; Lee, H. Y.; Lee, K. J. ROSics: Chemistry and Proteomics of Cysteine Modifications in Redox Biology. *Mass Spectrom. Rev.* **2015**, *34* (2), 184−208.
(79) Karoui, H.; Hogg, N.; Fréjaville, C.; Tordo, P.; Kalyanaraman, B. Characterization of Sulfur-Centered Radical Intermediates Formed during the Oxidation of Thiols and Sulfite by Peroxynitrite: ESR-SPIN Trapping and Oxygen Uptake Studies. *J. Biol. Chem.* **1996**, *271* (11), 6000−6009.
(80) Liu, K. J.; Miyake, M.; Panz, T.; Swartz, H. Evaluation of DEPMPO as a Spin Trapping Agent in Biological Systems. *Free Radic. Biol. Med.* **1999**, *26* (5−6), 714−721.
(81) Talukdar, R. Tracking down the Brominated Single Electron Oxidants in Recent Organic Red-Ox Transformations: Photolysis and Photocatalysis. *Org. Biomol. Chem.* **2020**, *18* (41), 8294−8345.
(82) Costentin, C.; Robert, M.; Savéant, J. M. Fragmentation of Aryl Halide π Anion Radicals. Bending of the Cleaving Bond and Activation vs Driving Force Relationships. *J. Am. Chem. Soc.* **2004**, *126* (49), 16051−16057.
(83) Zhang, L.; Israel, E. M.; Yan, J.; Ritter, T. Copper-Mediated Etherification via Aryl Radicals Generated from Triplet States. *Nat. Synth.* **2022**, *1* (5), 376−381.
(84) de Beus, M. D.; Chung, J.; Colón, W. Modification of Cysteine 111 in Cu/Zn Superoxide Dismutase Results in Altered Spectroscopic and Biophysical Properties. *Protein Sci.* **2004**, *13* (5), 1347−1355.
(85) Singh, S.; Hämäläinen, R. H. The Roles of Cystatin B in the Brain and Pathophysiological Mechanisms of Progressive Myoclonic Epilepsy Type 1. *Cells* **2024**, *13* (2), 170.
(86) Canarelli, S. E.; Swalm, B. M.; Larson, E. T.; Morrison, M. J.; Weerapana, E. Monitoring GAPDH Activity and Inhibition with Cysteine-Reactive Chemical Probes. *RSC Chem. Biol.* **2022**, *3* (7), 972.
(87) Tiwari, A.; Hayward, L. J. Familial Amyotrophic Lateral Sclerosis Mutants of Copper/Zinc Superoxide Dismutase Are Susceptible to Disulfide Reduction. *J. Biol. Chem.* **2003**, *278*, 5984−5992.
(88) Devarie-Baez, N. O.; Lopez, E. I. S.; Furdui, C. M. Biological Chemistry and Functionality of Protein Sulfenic Acids and Related Thiol Modifications. *Free Radic. Res.* **2016**, *50* (2), 172−194.
(89) Abdel-Wahab, M. H.; Arafa, H. M. M.; El-Mahdy, M. A.; Abdel-Naim, A. B. Potential Protective Effect of Melatonin against Dibromoacetonitrile-Induced Oxidative Stress in Mouse Stomach. *Pharmacol. Res.* **2002**, *46* (3), 287−293.
(90) Trichloroacetonitrile Properties—SpringerMaterials. https://materials.springer.com/substanceprofile/docs/smsid_ctxwtnkbzyoizvop (accessed Nov 5, 2024).
(91) Dichloro-Acetonitrile Properties—SpringerMaterials. https://materials.springer.com/substanceprofile/docs/smsid_cqgabjtledwitfky (accessed Nov 5, 2024).
(92) Dibromo-Acetonitrile Properties—SpringerMaterials. https://materials.springer.com/substanceprofile/docs/smsid_vfzukcnaqgzozrmq (accessed Nov 5, 2024).
(93) Bromoacetonitrile Properties—SpringerMaterials. https://materials.springer.com/substanceprofile/docs/smsid_oprnrjojvvwapmhr (accessed Nov 5, 2024).
(94) Iodoacetonitrile Properties—SpringerMaterials. https://materials.springer.com/substanceprofile/docs/smsid_inqumwkttzqqllud (accessed Nov 5, 2024).
(95) Chloroacetonitrile Properties—SpringerMaterials. https://materials.springer.com/substanceprofile/docs/smsid_xkmihdfcroyexcfa (accessed Nov 5, 2024).

https://doi.org/10.1021/acsenvironau.4c00068
ACS Environ. Au 2025, 5, 101−113